Hindawi Publishing Corporation
Journal of Polymers
Volume 2013, Article ID 162603, 10 pages
http://dx.doi.org/10.1155/2013/162603

Research Article

Structure/Property Relationships of Poly(L-lactic Acid)/Mesoporous Silica Nanocomposites

Javier Gudiño-Rivera,[1] Francisco J. Medellín-Rodríguez,[1] Carlos Ávila-Orta,[2] Alma G. Palestino-Escobedo,[1] and Saúl Sánchez-Valdés[2]

[1] *Facultad de Ciencias Químicas, CIEP-FCQ, Universidad Autónoma de San Luis Potosí, Avenida Dr. Manuel Nava Martínez 6, 78210 San Luis Potosí, SLP, Mexico*
[2] *Centro de Investigación en Química Aplicada, Boulevard Enrique Reyna 140, P.O. Box 379, 25100 Saltillo, COAH, Mexico*

Correspondence should be addressed to Francisco J. Medellín-Rodríguez; francmr@uaslp.mx

Received 29 June 2013; Revised 7 October 2013; Accepted 8 October 2013

Academic Editor: Zhong-Ming Li

Biodegradable poly(L-lactic acid) (PLLA)/mesoporous silica nanocomposites were prepared by grafting L-lactic acid oligomer onto silanol groups at the surface of mesoporous silica (SBA-15). The infrared results showed that the lactic acid oligomer was grafted onto the mesoporous silica. Surface characterization of mesoporous silica proved that the grafted oligomer blocked the entry of nitrogen into the mesopores. Thermal analysis measurements showed evidence that, once mixed with PLLA, SBA-15 not only nucleated the PLLA but also increased the total amount of crystallinity. Neat PLLA and its nanocomposites crystallized in the same crystal habit and, as expected, PLLA had a defined periodicity compared with the nanocomposites. This was because the grafted macromolecules on silica tended to cover the lamellar crystalline order. The g-SBA-15 nanoparticles improved the tensile moduli, increasing also the tensile strength of the resultant nanocomposites. Overall, the silica concentration tended to form a brittle material.

1. Introduction

Poly(L-lactic acid) (PLLA) is a linear aliphatic polyester widely used in biomedical applications because it is biodegradable, biocompatible, and nontoxic for the human body. It is also approved by the Food and Drug Administration (FDA) for applications in orthopedic devices [1]. Moreover, PLLA is used as scaffold for bone tissue regeneration [2–6]. However, its slow crystallization, slow degradation rates, low stability during degradation, and relatively poor mechanical properties have limited the applications of this polymer, in particular as a scaffold material [7].

Therefore, new applications for this polymer have proposed the preparation of nanocomposites with inorganic reinforcements as a convenient alternative [8, 9]. Some examples are PLLA nanocomposites with nanoclays [10, 11], nanohydroxyapatite [12, 13], carbon nanotubes [14, 15], and silicon dioxide [16, 17]. In general terms, the mechanical and thermal properties of the resultant nanocomposites have been improved, and the degree of crystallization, and hydrolytic degradation resistance has also been enhanced [14]. However, certain inorganic materials, such as carbon nanotubes [18], are considered to be toxic or harmful to cells.

A new class of polymeric materials, for which there are few published studies, takes advantage of mesoporous silicas. These are synthetic materials with ordered arrangements of channels and cavities of different geometries and siloxane walls. One example is SBA-15, a mesoporous material synthetized using triblock copolymer surfactant as a template under acidic conditions [19]. Mesoporous silicas have large pore diameters (5–30 nm), high surface area (600–1000 m^2/g) and exhibit highly ordered 2D hexagonal mesostructures with uniform cylindrical channels [20]. These characteristics represent an advantage of mesoporous silicas compared with other nonporous inorganic nanofillers. Furthermore, the pores of the mesoporous silicas can be filled up with the polymeric macromolecules, which promote the intimate interactions and physical stability between the polymer and the inorganic phase [21]. Vallet-Regí et al. [22] reported

in vitro studies that compared the bioactive behavior of SBA-15 with other mesoporous materials. This behavior was assigned to the presence of silanol groups on the SBA-15 surface, which acted as nucleation sites for the apatite formation [23]. Apatite was considered to be suitable for biomedical applications such as bone tissue regeneration [24].

Several synthesis methods have been developed to improve the interactions and the adhesion between the inorganic phase and the PLLA matrix. Some of the synthesis methods include surface coatings, coupling agents, and other additives. For example, Yan et al. [16] reported a surface modification method that used the grafting of L-lactic acid oligomer onto the surface of the silanol groups of silica nanoparticles using a condensation reaction with toluene. Grafting of SiO_2 nanoparticles into a PLLA matrix improved the toughness, tensile strength, and thermal properties of the products. However, the incorporation of nongrafted SiO_2 nanoparticles decreased the mechanical properties.

Wu et al. [25] prepared PLLA/SiO_2 nanocomposites via insitu melt polycondensation of L-lactic acid with acidic acidic silica sol to study the effect of SiO_2 nanoparticles on the melt polycondensation behavior. The results demonstrated that during the polycondensation process, the chemical grafting of L-lactic acid oligomer occurred on the SiO_2 nanoparticles surface, specifically on the silanol groups. In addition, the molecular weight of PLLA decreased with the increase in SiO_2 concentration in the reactor. Li et al. [26] prepared PLLA/PLLA-grafted SiO_2 nanocomposites using in situ melt polycondensation. The thermooxidative degradation process of nanocomposites with SiO_2 was examined and the results showed that the presence of grafted SiO_2 nanoparticles improved the stability of PLLA.

Considering the importance of PLLA as a biocompatible polymer and the use of a synthetic inorganic additive to generate new polymeric nanocomposites, in the present study, we prepared PLLA/gSBA-15 nanocomposites via solution mixing in chloroform as the common solvent. The main objectives were to study the grafting process and the crystallization, melting, and mechanical behavior of the resultant products.

2. Materials and Methods

2.1. Materials. PLLA (M_w = 100000 g/mol), was purchased from Polysciences Inc., and the L-lactic acid (85 wt% aqueous solution) was from Sigma-Aldrich. Pluronic P123 triblock copolymer (P123) was also from Sigma-Aldrich, and the tetraethylorthosilicate (TEOS) was from Fluka Inc.

2.2. Mesoporous Silica Synthesis. SBA-15 silicas were synthesized as reported by Zhao et al. [19] using 4.0 g sample of P123 as the template. The triblock copolymer was dissolved in water and 120 g of 2 M HCl solution. Then, 8.5 g of TEOS was added as the silica source. The mixture was maintained at 35°C for 24 h with stirring and at 100°C for 24 h without stirring. The solid product was filtered, washed with water, and subjected to a hydrothermal treatment at 100°C under stirring. This procedure was done to increase the hydrothermal stability of mesoporous silicas during the polycondensation reaction [27]. The resultant product was filtered and dried in an oven at 90°C overnight. Subsequently, it was oxidized in air for 3 h at 250°C followed by 4 h at 550°C.

2.3. Grafting of Lactic Acid Oligomer on the Surface of Mesoporous Silica. The lactic acid oligomer was grafted on the surface of the mesoporous silicas through a polycondensation reaction of L-lactic acid without any catalyst [28, 29]. Once the mesoporous silica was incorporated into the L-lactic acid solution (2.5 wt%), the mixture was ultrasounded to obtain a uniform suspension. Next, the mixture was dehydrated at 150°C and atmospheric pressure for 2 h at a reduced pressure of 100 torr for 2 h and again under pressure of 30 torr for 4 h. Subsequently, the reaction mixture was cooled to room temperature. The lactic acid oligomer grafted mesoporous silica (g-SBA-15) was separated by centrifugation and washed with chloroform to completely remove the free oligomer. Next, the product was dried in an oven at 70°C over-night to remove the residual chloroform.

2.4. Preparation of PLLA/SBA-15 and PLLA/g-SBA-15 Nanocomposites. PLLA/SBA-15 and PLLA/g-SBA-15 nanocomposites were prepared via solution mixing using chloroform as a solvent. The appropriate amount of grafted or nongrafted SBA-15 (5, 10, and 15 wt/wt%) was dispersed in chloroform using ultrasound. The PLLA samples were diluted in chloroform and stirred at 70°C for 1 h to complete the dissolution process. Next, the PLLA solution was added to the silica suspension under ultrasound with stirring. In the final step, the PLLA/silica solution was poured into a dish to evaporate the solvent at room temperature and was dried at 70°C overnight.

2.5. Characterization. FTIR measurements were performed in a Bruker Vector 22 spectrophotometer in attenuated total reflectance (ATR) mode to characterize the neat L-lactic acid oligomer, and SBA-15 and to monitor the g-SBA-15 formation. Nitrogen adsorption-desorption measurements were performed in a Micromeritics ASAP2020 gas adsorption analyzer at 77°K. The samples surface area was calculated using the Brunauer-Emmett-Teller (BET) method [30] in the relative pressure range of P/P_0 = 0.02–0.3. The pore size distributions were calculated from the desorption branch using the Barrett-Joyner-Halenda (BJH) model [31], and the pore size was calculated from the peak position of the distribution curve. The pore volume was measured at the P/P_0 = 0.999 position. The thermal analyses were performed in a Perkin Elmer DSC-7 calorimeter. The temperature scans were performed at a heating rate of 10°C/min. For nonisothermal melt crystallization, the samples were heated from room temperature to 200°C; then they were cooled to 20°C. These samples were further heated from room temperature to 200°C to register the melting trace. The crystallization temperature (T_c) was obtained from the first cooling traces. The melting temperature (T_m) and the melting enthalpy (ΔH_m) of the neat PLLA and its composites were measured from the second heating trace. For the isothermal crystallization measurements, the corresponding samples were crystallized at a crystallization temperature of 120°C for 30 min. In the

final step, the studied samples were heated up from the crystallization temperature to 200°C. An optical polarized microscope (POM) (Olympus BX60), equipped with a temperature controller (Mettler FP90), and two Mettler FP82HT hot stages were used to register morphological changes. In order to erase the thermal history, the studied samples were first melt at 200°C for 3 min and then quickly transferred to the crystallization stage set at 120°C. For the WAXD measurement, the samples of PLLA and its nanocomposites were crystallized at a temperature of 120°C, where they remained for 30 min before being quenched. The WAXD patterns were obtained in a PANalytical X'pert Pro X-ray diffractometer. The Cu Kα radiation source (λ = 1.5418 Å) was operated with an accelerating voltage of 35 kV. The range of the diffracting 2θ angle was 5–40°, and the scanning rate was 10°/min. This experimental technique was used to identify the crystalline structure of PLLA, its evolution after the nanocomposite preparation, and the crystallization degree of samples. The SAXS experiments were performed in a NanoStar Bruker SAXS instrument using an accelerating voltage of 40 kV and a current intensity of 35 mA. The sample to detector distance was 1.1 m and the Cu/Kα X-ray radiation (λ = 1.5418 Å) was used as the X-ray source. In this case, powder specimens of SBA-15 and g-SBA-15 were used with an exposure time of 600 s for all samples. The tensile tests were performed in an Instron 365 machine at a crosshead speed of 10 mm/min, at 23 ± 2°C. All of the composite films were cut into specimens with constant dimensions (28 mm × 9 mm × 0.25 mm).

3. Results and Discussion

3.1. Surface Grafting Reaction. FTIR was used to qualitatively monitor the surface grafting reaction, assuming that the expected amount of grafting was above the experimental detection limits of this technique. Figure 1(a) shows the FTIR spectrum of SBA-15 before grafting, in which the typical Si–O–Si vibration bands, which are related to the peak positions of 1068 and 806 cm^{-1}, are associated with the condensed silica network. In addition, there are a vibration band at 966 cm^{-1}, which is attributed to Si–OH stretching of the free surface silanols groups [32], and a broad band between 3750 and 3000 cm^{-1}, which is in the OH stretching vibrational region. Figure 1(b) shows the FTIR reference vibration pattern of the L-lactic acid oligomer, which was used to chemically modify SBA-15 nanoparticles. Figure 1(c) shows the spectrum of SBA-15 after grafting, where the results show new absorption bands at 1759 cm^{-1}, 2946 cm^{-1}, and 2999 cm^{-1}, as a consequence of the grafting reaction. These absorption bands are assigned to the carbonyl group (C=O) and the C–H stretching vibrations of the L-lactic acid oligomer grafted on the surface of SBA-15 nanoparticles. In quantitative terms, the ratio between the peak intensities indicated the average levels of 6% grafting. Considering the FTIR results, a surface modification reaction mechanism of mesoporous silica is shown in Scheme 1, where the polycondensation reaction conditions are also specified. According to Scheme 1, under oligomerization conditions, the silanol groups on mesoporous mesoporous silica react with the carbonyl groups of the L-lactic acid monomer and release water.

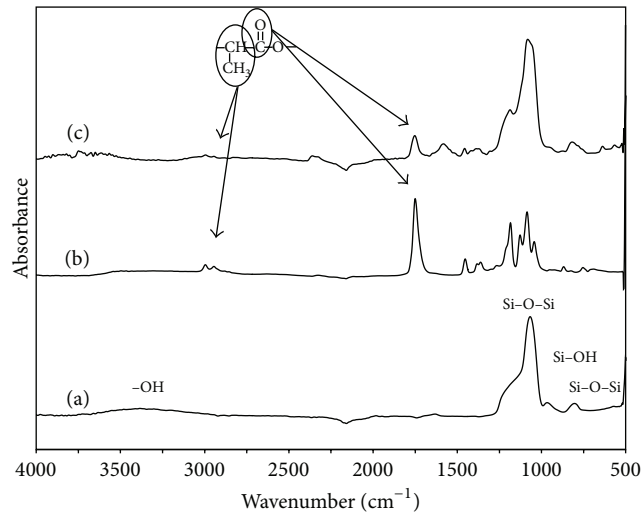

Figure 1: FTIR spectra of (a) SBA-15, (b) L-lactic acid oligomer (OLLA), and (c) g-SBA-15.

Table 1: Physical properties of SBA-15 before and after grafting.

Material	Surface area (m^2g^{-1})	Pore diameter (nm)	Pore volume (cm^3g^{-1})
SBA-15	678	5.9	0.90
g-SBA-15	41	4.9	0.10

As a result, the oligomer is grafted onto the surface of mesoporous silica. Li et al. [17] reported the preparation of PLLA/PLLA-grafted SiO_2 nanocomposites by in situ melt polycondensation. In contrast, we confirmed the grafting reaction after the oligomerization stage. This reaction occurred without using catalysts during the polycondensation reaction, although the condensed water was removed while the vacuum and the temperature were progressively increased. This removal is a stage in which the low molecular weight PLLA is produced, according to the melt polycondensation process of PLLA which was proposed by Moon et al. [28].

To understand the structure/property relation of the resultant nanocomposites, nitrogen adsorption measurements were performed to measure the porosity of mesoporous silicas before and after grafting. The structural parameters derived from the adsorption data are listed in Table 1, where the results of specific surface area and pore volume of nongrafted and grafted SBA-15 showed a marked decrease. These results indicated that the original surface area of mesoporous silica was covered with oligomer molecules, which restricted the access of nitrogen into the pores of SBA-15.

In agreement with our results, Moller et al. [33] reported the synthesis of composites of poly(methyl methacrylate) (PMMA) with the mesoporous silicas MCM-41 and MCM-48. After polymerization, the mesopores were blocked, and the surface area and pore volume of both materials were significantly reduced. Additionally, it is expected that

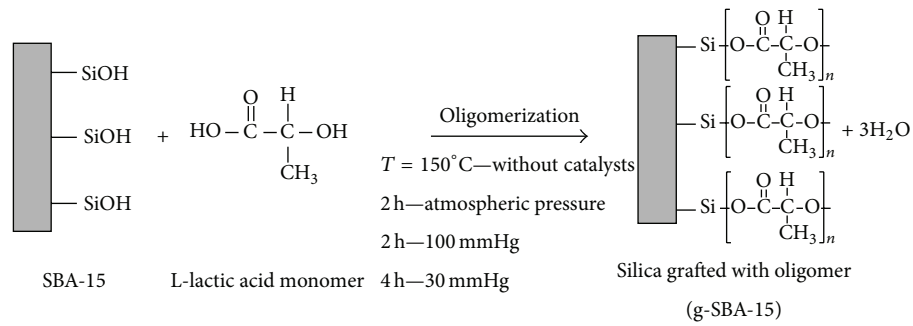

Scheme 1: Surface modification reaction of mesoporous silicas.

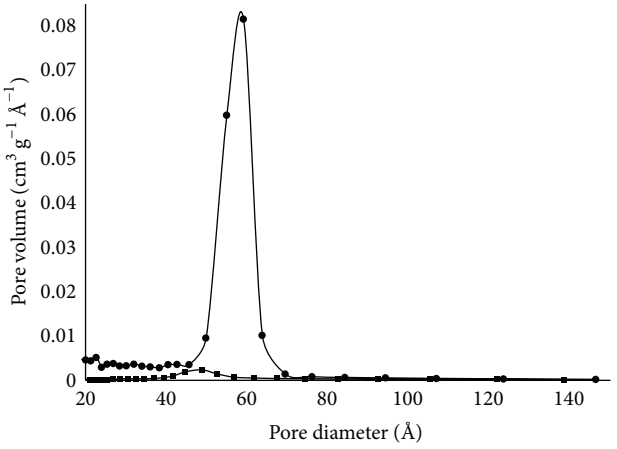

Figure 2: Pore size distributions for SBA-15 mesoporous silicas (•) and g-SBA-15 (■).

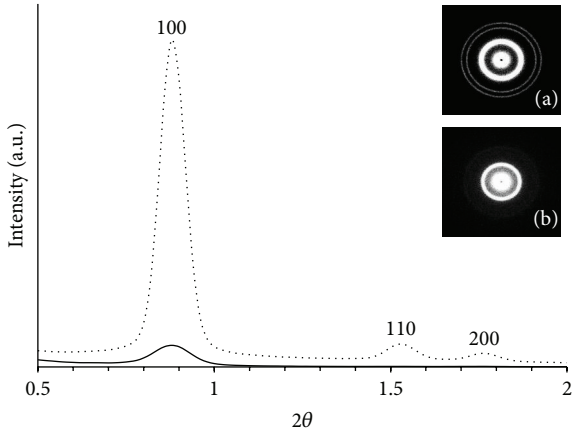

Figure 3: 1D SAXD patterns (dotted line: SBA-15, solid line: g-SBA-15). Insets: (a) 2D SAXD image of SBA-15, (b) 2D SAXD image g-SBA-15.

a surface modified material with lactic acid oligomer has greater affinity with the organic polymeric PLLA matrix than that with the unmodified material, resulting in a better dispersion of the grafted material.

The pore sizes were estimated from the peak positions of the BJH desorption pore size distribution curves. SBA-15 shows a narrow pore distribution in Figure 2, which correspond to an average diameter of 59 Å (5.9 nm). Meanwhile, g-SBA-15 (see also Figure 2) showed a slightly broader distribution and a lower intensity with an average diameter of 49 Å (4.9 nm), indicating less ordered pore structure.

These results illustrate that the oligomer molecules, which are grafted onto the surface of mesoporous silicas after the polycondensation reaction, block the pores decreasing the average pore size diameter of the resultant product. The decrease in the maximum intensity and the increase in its width also imply an increase in the pore heterogeneity in the grafted material compared with the nongrafted silica.

Small-angle X-ray diffraction (SAXD) patterns, that is, assuming a diffraction effect, of SBA-15 and g-SBA-15, are shown in Figure 3.

The scattering vector q is generally employed in SAXS analyses, which is related to the diffraction angle (θ) using the Bragg equation ($\lambda = 2d \sin\theta$) with $q = 4\pi \sin\theta/\lambda$, where $\lambda = 1.5418$ Å. However, we have used a SAXS system to obtain the diffraction patterns of silicas in terms of the diffracting angle. According to Figure 3, there are three resolved reflections in the nongrafted SBA-15, which can be indexed as [100], [110], and [200] and which emerge from a hexagonal mesostructure [19].

Table 2: SAXD data of SBA-15 before and after grafting.

Material	d_{100} [a] (nm)	d_{110} [a] (nm)	d_{200} [a] (nm)
SBA-15	10.0	5.8	5.0
g-SBA-15	10.0	—	—

[a] d values of reflections ($d_{hkl} = \lambda/2 \sin\theta$).

In the grafted g-SBA-15, all of the peak intensities became attenuated (see also Figure 3). The SBA-15 2D SAXD image (inset (a)) shows three well-defined concentric rings. However, in g-SBA-15 (inset (b)), the SAXD pattern appears attenuated, and the outer reflections became extinct and did not show any crystal orientation. This result occurred because the amorphous oligomer is grafted on the surface of the mesoporous silica, which impedes the detection of crystal reflections from the SBA-15 crystalline structure. Therefore, these results agree with the N_2 adsorption-desorption results that were discussed before. The values of the d spacing (i.e., position of diffracting planes) of the nongrafted and grafted silicas are shown in Table 2, where it is observed that both

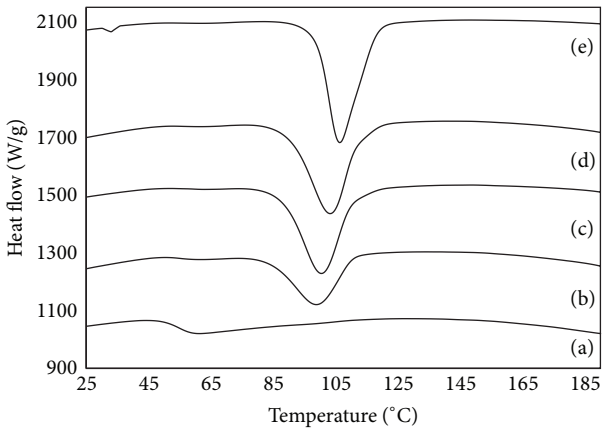

Figure 4: Nonisothermal melt crystallization: first cooling. (a) Neat PLLA, (b) nongrafted SBA-15 (5 wt%), (c) g-SBA-15 (5 wt%), (d) g-SBA-15 (10 wt%), and (e) g-SBA-15 (15 wt%).

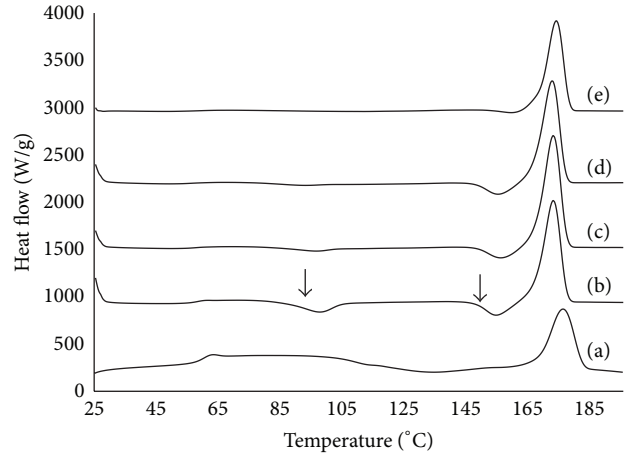

Figure 5: Nonisothermal melt crystallization and the subsequent melting traces: second heating. (a) Neat PLLA, (b) nongrafted SBA-15 (5 wt%), (c) g-SBA-15 (5 wt%), (d) g-SBA-15 (10 wt%), and (e) g-SBA-15 (15 wt%).

materials have similar values for the measurable reflections, indicating the periodic structure preservation of mesoporous silica after surface modification.

3.2. Crystallization and Melting Behavior of PLLA and Its Nanocomposites. To determine the morphological changes as a function of temperature, the nonisothermal melt crystallization, followed by the melting of the neat PLLA and its nanocomposites was performed by DSC. Figure 4 shows the DSC thermal traces of the samples, which were cooled from the melt at 10°C/min (first cooling). In this particular case, the results show that the incorporation of SBA-15 and g-SBA-15 significantly alters the nonisothermal melt crystallization of PLLA.

This effect is well known as heterogeneous nucleation [34] and has several particular characteristics in the context of the present study. First, it is noticed that nongrafted SBA-15 not only nucleates PLLA but also increases the amount of crystallization (see also Table 3). Furthermore, mesoporous grafted silica (i.e., g-SBA-15) strongly enhances nucleation and crystallinity (the area under the crystallization curve); these effects are proportional to silica concentration. These results can be explained considering that g-SBA-15 is covered with similar chemical structure as PLLA, as previously shown in Scheme 1. Therefore, due to molecular contact, g-SBA-15 is a better nucleating agent than SBA-15. In agreement with these results, Yan et al. [16] reported that g-SiO_2 nanoparticles act as nucleating agents for the PLLA crystallization, increasing its crystallinity with the g-SiO_2 content. Lu et al. [35] reported however a lower crystallinity of the PLLA matrix after increasing the amount of grafted TiO_2 particles. This was considered due to the lower mobility of the polymeric chains and their crystallization ability. Compared with such study, we observed the opposite behavior, an increase in the value of the degree of crystallinity (area under the cooling trace; see also Table 3), particularly when a higher content of g-SBA-15 is added to the system. The subsequent melting of PLLA and its nanocomposites after cooling from the melt at 10°C/min (second heating) is shown in Figure 5, where a rather complex evolution is involved in the results. In particular, nongrafted SBA-15 motivated the formation of two crystallization heating exotherms (see the arrows in Figure 5) and a main melting endotherm.

Table 3: DSC and WAXD results of PLLA and its nanocomposites.

g-SBA-15 content (wt%)	T_m (°C)	Crystallinity of PLLA[b] (%)
0	180.1	30.7
5[a]	176.0	33.6
5	176.8	29.2
10	177.3	29.8
15	177.8	27.9

[a]Nongrafted.
[b]Determined by WAXD.

However, g-SBA-15 promoted a different behavior, that is, tending to decrease the exotherms until their complete disappearance (see curves (c), (d), and (e) in Figure 5). Medellín-Rodríguez et al. [36] suggested an explanation for the exotherm before melting in Nylon 6 that involved a recrystallization process, that is, an increase in the lamellar thickness, which is associated with the late stages of recrystallization before melting. Here, the results show that the grafted g-SBA-15 stabilizes the crystalline structure in such a manner that it cannot recrystallize.

It is important to mention that the melting point (T_m) values of all of the nanocomposites are lower than those of the reference neat PLLA, although such values slightly increase with the content of grafted mesoporous silicas (see also Table 3). This result suggests that crystals in the neat PLLA, although in less quantity, are more perfect than those in the other cases, where the imperfection emerges from the interactions in different proportions with the g-SBA15 substrates.

The melting traces after the isothermal crystallization of the neat PLLA and its composites are shown in Figure 6. In this case, we performed all of the experiments at the same

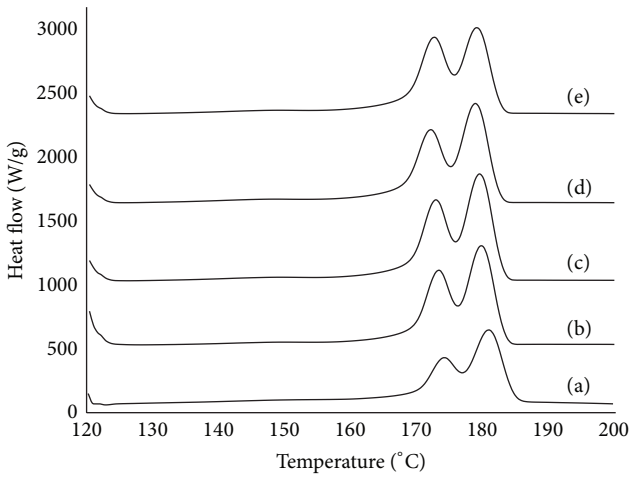

Figure 6: Isothermal crystallization and the subsequent melting traces. (a) Neat PLLA, (b) nongrafted SBA-15 (5 wt%), (c) g-SBA-15 (5 wt%), (d) g-SBA-15 (10 wt%), and (e) g-SBA-15 (15 wt%).

scanning rate (10°C/min), under identical crystallization conditions. The results in Figure 6 show a double-melting behavior and the influence of the silica content. The first low endotherm increased when SBA-15 was added into the system and it continued to grow proportionally with the g-SBA-15 content.

If we assume that the first melting endotherm is associated with secondary crystals [37], then the formation of such crystals is enhanced by both the incorporation of SBA-15 and that of g-SBA-15.

3.3. Spherulitic Morphology of PLLA and Its Nanocomposites. The spherulitic morphology of PLLA and the effects of incorporation of mesoporous silicas were determined by polarized optical microscopy. Figure 7(a) shows the spherulitic morphology of neat PLLA after several periods of isothermal crystallization (1, 5, and 15 min) at 120°C. In this case, well-developed, heterogeneous size spherulites are observed with a large amount of amorphous areas. Figures 7(b) and 7(c) show the corresponding POM micrographs of nongrafted (PLLA/SBA-15) and grafted (PLLA/g-SBA-15) nanocomposites. In this case, the overall size of spherulites became smaller with the incorporation of SBA-15, a typical effect of heterogeneous nucleation, as proposed before. In addition, few amorphous areas are still observed. Once the g-SBA-15 is incorporated (Figure 7(c)), a higher nucleation effect is observed with very small crystalline entities and the absence of amorphous areas.

3.4. Crystalline Structure of PLLA and Its Nanocomposites. At this stage, it was necessary to analyze the crystallization evolution of the studied samples in terms of X-ray diffraction. Figure 8 illustrates the normalized diffraction patterns of PLLA and its nanocomposites. These images were obtained after isothermal crystallization at 120°C during 30 minutes. It is shown that both PLLA and their nanocomposites crystallized into the stable α crystalline form [38]. Therefore, all of the samples showed the main characteristic diffracting peaks at the 2θ positions 12.4°, 14.7°, 16.9°, 19.1°, and 22.4°, which correspond to the diffracting planes [101], [010]; [110]; and [200], [111]; and [201], [102], and [210], respectively [38]. In summary, these results show the same diffraction patterns in all of the samples, which implies that the incorporation of mesoporous silicas did not modify the crystal structure of PLLA.

Considering the thermal effects that calculation of crystallinity involves in DSC, it was necessary to calculate the crystallinity values from the WAXD measurements. The crystallinity of the studied samples is shown in Table 3, where it is indeed observed that the amount of crystallinity depends on the presence, amount, and nature of SBA-15. In particular, it increases with the grafting of SBA-15.

A different option was studied using SAXS, that is, the evolution of morphological periodicities. The corresponding SAXS patterns of all of the studied samples are shown in Figure 9, where the scattering maximum indicates the crystals periodicity. The results show that the integration of nongrafted SBA-15 attenuated the crystalline periodicity, indicating that the system became morphologically disordered as a consequence of the SBA-15 integration. The periodicity is also known as the long period (L), which can be obtained from the Lorentz corrected plot of intensity versus the scattering vector q using the equation [39]

$$L = \frac{2\pi}{q_{\max}}. \quad (1)$$

In the neat PLLA, the value of $q_{\max}$ was 0.313 nm^{-1}; therefore, L = 20.08 nm which is an average value of periodicity in semicrystalline polymers. With respect to the evolution of g-SBA-15, its pattern gradually became attenuated with the concentration because the grafting effect also distorted the definition of the original crystal periodicity.

3.5. Mechanical Properties. Figure 10 shows typical stress-strain curves, together with their standard deviation, of neat PLLA and its nanocomposites with different silica contents. The results of the PLLA and PLLA/SBA-15 nanocomposites exhibited a ductile behavior, that is, an elastic region followed by nonlinear deformation, which was followed by plastic deformation at a constant load before breaking. The difference in strain at break between PLLA and PLLA/SBA-15 must be due to the lower amount of rubbery ductile amorphous areas in this last case, as shown in Figure 7. The elastic modulus of the PLLA/SBA-15 mixture (Table 4) was more than 2 times higher than that of the neat PLLA. Therefore, mesoporous silica can be considered a mechanical reinforcement for this polymeric system. Furthermore, the PLLA surface-grafted g-SBA-15 (5 wt%) nanocomposites exhibited lower ductility (Figure 10) and higher tensile strength at yield but similar tensile modulus as PLLA/SBA-15 nanocomposites.

The explanation for this behavior can be assigned to the nucleation effect, which morphologically decreases the amount of amorphous rubbery material (see Figure 7) and also increases the number of crystals. The main consequence

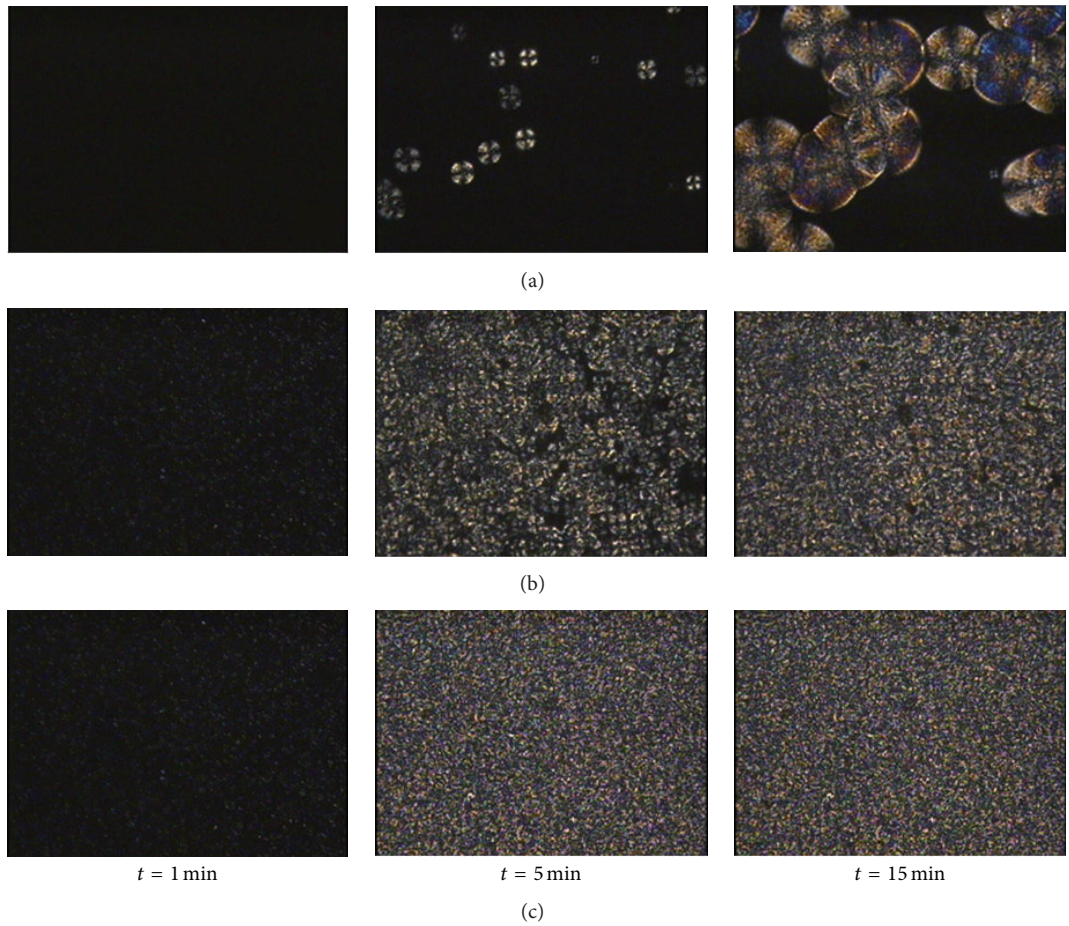

Figure 7: Spherulitic morphologies of (a) neat PLLA, (b) nongrafted SBA-15 (5 wt%), and (c) g-SBA-15 (5 wt%) crystallized at 120°C.

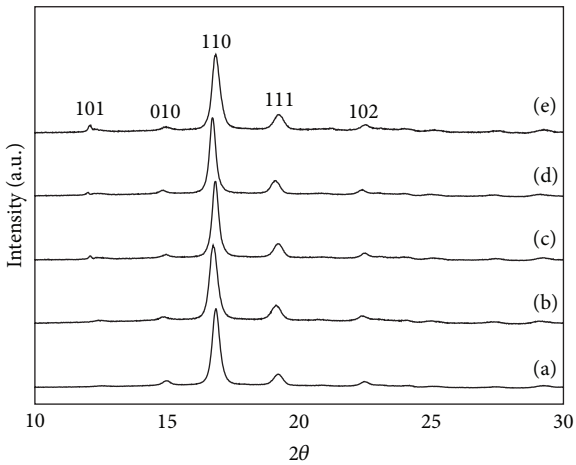

Figure 8: WAXD patterns of (a) neat PLLA, (b) nongrafted SBA-15 (5 wt%), (c) g-SBA-15 (5 wt%), (d) g-SBA-15 (10 wt%), and (e) g-SBA-15 (15 wt%).

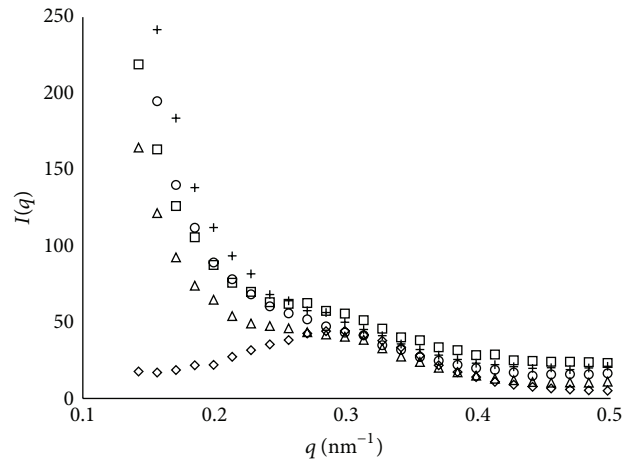

Figure 9: 1D SAXS patterns (◊) neat PLLA, (□) nongrafted SBA-15 (5 wt%), (△) g-SBA-15 (5 wt%), (∘) g-SBA-15 (10 wt%), and (+) g-SBA-15 (15 wt%).

is that the amount of crystal interfaces rises, due to the high number of nuclei, resulting in a more brittle material (see also Table 4).

The stress-strain curves of the nanocomposites gradually displayed the characteristics of brittle materials when the g-SBA-15 content increased. In particular, the tensile strength

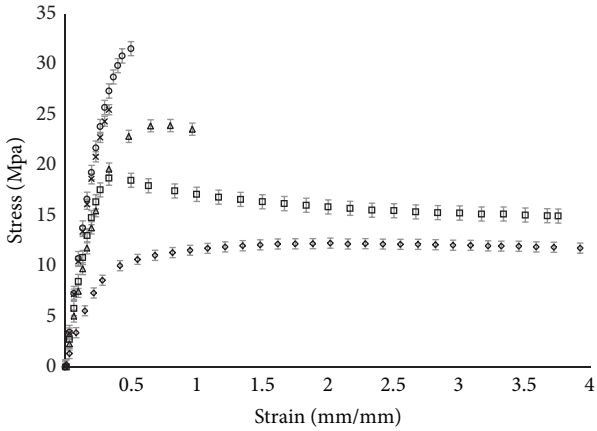

Figure 10: Stress-strain curves of (◊) neat PLLA, (□) nongrafted SBA-15 (5 wt%), (△) g-SBA-15 (5 wt%), (∘) g-SBA-15 (10 wt%), and (+) g-SBA-15 (15 wt%).

Table 4: Mechanical properties of PLLA and its composites.

g-SBA-15 content (wt%)	Tensile strength (MPa)	Maximum strain (mm/mm)	Modulus (Mpa)
0	12.3	3.9	10.3
5[a]	18.9	3.7	24.8
5	23.9	1.0	22.8
10	31.5	0.5	28.0
15	25.5	0.3	27.3

[a]Nongrafted.

of the PLLA/g-SBA-15 (10 wt%) attained a maximum value of tensile strength and slightly higher modulus than PLLA/g-SBA-15 (15 wt%). This is typical of a system that gradually incorporates a rigid phase; that is, the system becomes mechanically weaker.

The disparity in mechanical properties in Figure 10 is a manifestation of the morphological changes that occur in every polymeric system. The tendency in the results of the neat PLLA does not correspond to that of a semicrystalline polymer and the most probable reason is the lower crystallinity of PLLA compared to the other polymers. For the low concentration (5 wt%) PLLA/SBA-15 mixture, the increase in nucleation and crystallinity, which was previously discussed, promoted the formation of spherulites, which rendered the expected pattern deformation of semicrystalline polymers [40]. With respect to grafted g-SBA15, although nucleation increased, the mechanical deformation was no longer typical of spherulites deformation. There was a clear tendency to the formation of a brittle material, which most likely originated from the substrate integration that must have generated a morphological change that was no longer associated with spherulites. This behavior maintained its tendency until a true brittle material was formed, because the mesoporous silica phase was added, and the tensile strength was consequently decreased.

Ji et al. [41] reported the synthesis of poly((3-trimethoxysilyl) propyl methacrylate)/silica nanocomposites and the resultant products presented an increase in tensile strength and tensile modulus with the silica concentration, which agrees with our results. Therefore, mesoporous silicas were considered adequate to reinforce and toughen polymers.

4. Conclusions

L-lactic acid oligomer was grafted onto the surface of mesoporous silica (SBA-15) nanoparticles to create new synthetic and biodegradable polymeric systems. Lower nitrogen adsorption was detected in g-SBA-15 because the grafted oligomer molecules covered the mesopores of the original SBA-15. It was determined that g-SBA-15 had a similar diffraction pattern to the reference SBA-15 although the diffracting peak intensity was attenuated in the first case because the L-lactic oligomer was grafted onto the surface of the mesoporous silicas. Nonisothermal crystallization DSC measurements demonstrated that, because of the organic molecular characteristics, the grafted SBA-15 was highly efficient as a nucleating agent compared with the nongrafted SBA-15. The analyses of the melting behavior of the nanocomposites indicated that g-SBA-15 did interfere with the molecular mobility and as a consequence with the crystallization ability. Similar to the case of the other additives, the secondary crystallization, which is generally associated with the first of the two melting endotherms, proportionally increased with the amount of g-SBA15. Spherulitic crystals were formed in all of the composites, although the presence of nongrafted and grafted SBA-15 motivated a morphological change in the system as a consequence of a high heterogeneous nucleation. The integration of nongrafted SBA-15 attenuated the crystalline periodicity, which lead to the conclusion that the system became morphologically disordered as a consequence of the SBA-15 integration. Considering that surface-grafted g-SBA-15 (5 wt%) nanocomposites exhibited lower ductility than SBA-15, it was concluded that the nucleation effect decreased the amount of amorphous rubbery material and also increased the amount of crystal interfaces rises, resulting in a more brittle material. Overall, mesoporous silicas were considered to be suitable to reinforce and toughen PLLA.

Acknowledgments

This study was supported by CONACYT México through Grant 57070. J. Gudiño-Rivera thanks CONACYT for the scholarship 21496. The authors thank SEP-PIFI funding and CA213.

References

[1] J. C. Middleton and A. J. Tipton, "Synthetic biodegradable polymers as orthopedic devices," *Biomaterials*, vol. 21, no. 23, pp. 2335–2346, 2000.

[2] P. A. Gunatillake, R. Adhikari, and N. Gadegaard, "Biodegradable synthetic polymers for tissue engineering," *European Cells and Materials*, vol. 5, pp. 1–16, 2003.

[3] X. Liu and P. X. Ma, "Polymeric scaffolds for bone tissue engineering," *Annals of Biomedical Engineering*, vol. 32, no. 3, pp. 477–486, 2004.

[4] A. J. Salgado, O. P. Coutinho, and R. L. Reis, "Bone tissue engineering: state of the art and future trends," *Macromolecular Bioscience*, vol. 4, no. 8, pp. 743–765, 2004.

[5] A. Mistry and A. Mikos, "Advances in biochemical engineering," in *Regenerative Medicine II*, vol. 94, pp. 1–22, 2005.

[6] R. van Dijkhuizen-Randersma, L. Moroni, A. van Apeldoorn, Z. Zhang, and D. Grijpma, "Degradable polymers for tissue engineering," in *Tissue Engineering*, C. van Blitterswijk, Ed., pp. 193–221, Elsevier Academic Press, London, UK, 2008.

[7] K. van de Velde and P. Kiekens, "Biopolymers: overview of several properties and consequences on their applications," *Polymer Testing*, vol. 21, no. 4, pp. 433–442, 2002.

[8] F. Hussain, M. Hojjati, M. Okamoto, and R. E. Gorga, "Review article: polymer-matrix nanocomposites, processing, manufacturing, and application: an overview," *Journal of Composite Materials*, vol. 40, no. 17, pp. 1511–1575, 2006.

[9] I. Armentano, M. Dottori, E. Fortunati, S. Mattioli, and J. M. Kenny, "Biodegradable polymer matrix nanocomposites for tissue engineering: a review," *Polymer Degradation and Stability*, vol. 95, no. 11, pp. 2126–2146, 2010.

[10] S. I. Marras, I. Zuburtikudis, and C. Panayiotou, "Nanostructure versus microstructure: morphological and thermomechanical characterization of poly(l-lactic acid)/layered silicate hybrids," *European Polymer Journal*, vol. 43, no. 6, pp. 2191–2206, 2007.

[11] L. H. Lin, H. J. Liu, and N. K. Yu, "Morphology and thermal properties of poly(L-lactic acid)/organoclay nanocomposites," *Journal of Applied Polymer Science*, vol. 106, no. 1, pp. 260–266, 2007.

[12] X. Qiu, Z. Hong, J. Hu, L. Chen, X. Chen, and X. Jing, "Hydroxyapatite surface modified by L-lactic acid and its subsequent grafting polymerization of L-lactide," *Biomacromolecules*, vol. 6, no. 3, pp. 1193–1199, 2005.

[13] C. Y. Zhang, H. Lu, Z. Zhuang, X. P. Wang, and Q. F. Fang, "Nano-hydroxyapatite/poly(L-lactic acid) composite synthesized by a modified in situ precipitation: preparation and properties," *Journal of Materials Science*, vol. 21, no. 12, pp. 3077–3083, 2010.

[14] Y. Zhao, Z. Qiu, and W. Yang, "Effect of functionalization of multiwalled nanotubes on the crystallization and hydrolytic degradation of Biodegradable poly(L-lactide)," *Journal of Physical Chemistry B*, vol. 112, no. 51, pp. 16461–16468, 2008.

[15] G.-X. Chen, H.-S. Kim, B. H. Park, and J.-S. Yoon, "Controlled functionalization of multiwalled carbon nanotubes with various molecular-weight poly(L-lactic acid)," *Journal of Physical Chemistry B*, vol. 109, no. 47, pp. 22237–22243, 2005.

[16] S. Yan, J. Yin, Y. Yang, Z. Dai, J. Ma, and X. Chen, "Surface-grafted silica linked with l-lactic acid oligomer: a novel nanofiller to improve the performance of biodegradable poly(l-lactide)," *Polymer*, vol. 48, no. 6, pp. 1688–1694, 2007.

[17] D. Li, G. Liu, L. Wang, and Y. Shen, "Preparation and thermo-oxidative degradation of poly(L-lactic acid)/poly(L-lactic acid)-grafted SiO_2 nanocomposites," *Polymer Bulletin*, vol. 67, no. 8, pp. 1529–1538, 2011.

[18] M. Bottini, S. Bruckner, K. Nika et al., "Multi-walled carbon nanotubes induce T lymphocyte apoptosis," *Toxicology Letters*, vol. 160, no. 2, pp. 121–126, 2006.

[19] D. Zhao, Q. Huo, J. Feng, B. F. Chmelka, and G. D. Stucky, "Nonionic triblock and star diblock copolymer and oligomeric sufactant syntheses of highly ordered, hydrothermally stable, mesoporous silica structures," *Journal of the American Chemical Society*, vol. 120, no. 24, pp. 6024–6036, 1998.

[20] F. Zhang, Y. Yan, H. Yang et al., "Understanding effect of wall structure on the hydrothermal stability of mesostructured silica SBA-15," *Journal of Physical Chemistry B*, vol. 109, no. 18, pp. 8723–8732, 2005.

[21] L. Wei, N. Hu, and Y. Zhang, "Synthesis of polymer-mesoporous silica nanocomposites," *Materials*, vol. 3, no. 7, pp. 4066–4079, 2010.

[22] M. Vallet-Regí, L. Ruiz-González, I. Izquierdo-Barba, and J. M. González-Calbet, "Revisiting silica based ordered mesoporous materials: medical applications," *Journal of Materials Chemistry*, vol. 16, pp. 26–31, 2006.

[23] M. Vallet-Regí, M. Colilla, and I. Izquierdo-Barba, "Bioactive mesoporous silicas as controlled delivery systems: application in bone tissue regeneration," *Journal of Biomedical Nanotechnology*, vol. 4, no. 1, pp. 1–15, 2008.

[24] I. Izquierdo-Barba, M. Colilla, and M. Vallet-Regí, "Nanostructured mesoporous silicas for bone tissue regeneration," *Journal of Nanomaterials*, vol. 2008, Article ID 106970, 14 pages, 2008.

[25] L. Wu, D. Cao, Y. Huang, and B.-G. Li, "Poly(l-lactic acid)/SiO_2 nanocomposites via in situ melt polycondensation of l-lactic acid in the presence of acidic silica sol: preparation and characterization," *Polymer*, vol. 49, no. 3, pp. 742–748, 2008.

[26] D. Li, G. Lu, L. Wang, and Y. Shen, "Preparation and thermo-oxidative degradation of poly(l-lactic acid)/poly(l-lactic acid)-grafted SiO_2 nanocomposites," *Polymer Bulletin*, vol. 67, no. 8, pp. 1529–1538, 2011.

[27] L. Chen, T. Horiuchi, T. Mori, and K. Maeda, "Postsynthesis hydrothermal restructuring of M41S mesoporous molecular sieves in water," *Journal of Physical Chemistry B*, vol. 103, no. 8, pp. 1216–1222, 1999.

[28] S. I. Moon, C. W. Lee, M. Miyamoto, and Y. Kimura, "Melt polycondensation of L-lactic acid with Sn(II) catalysts activated by various proton acids: a direct manufacturing route to high molecular weight Poly(L-lactic acid)," *Journal of Polymer Science A*, vol. 38, no. 9, pp. 1673–1679, 2000.

[29] F. Achmad, K. Yamane, S. Quan, and T. Kokugan, "Synthesis of polylactic acid by direct polycondensation under vacuum without catalysts, solvents and initiators," *Chemical Engineering Journal*, vol. 151, no. 1–3, pp. 342–350, 2009.

[30] J. Rouquerol, D. Avnir, C. W. Fairbridge et al., "Recommendations for the characterization of porous solids," *Pure and Applied Chemistry*, vol. 66, no. 8, pp. 1739–1758, 1994.

[31] M. Kruk, M. Jaroniec, C. H. Ko, and R. Ryoo, "Characterization of the porous structure of SBA-15," *Chemistry of Materials*, vol. 12, no. 7, pp. 1961–1968, 2000.

[32] B. A. Morrow and A. J. McFarlan, "Chemical reactions at silica surfaces," *Journal of Non-Crystalline Solids*, vol. 120, no. 1–3, pp. 61–71, 1990.

[33] K. Moller, T. Bein, and R. X. Fischer, "Entrapment of PMMA polymer strands in microand mesoporous materials," *Chemistry of Materials*, vol. 10, no. 7, pp. 1841–1852, 1998.

[34] J. H. Lee, T. G. Park, H. S. Park et al., "Thermal and mechanical characteristics of poly(L-lactic acid) nanocomposite scaffold," *Biomaterials*, vol. 24, no. 16, pp. 2773–2778, 2003.

[35] X. Lu, X. Lv, Z. Sun, and Y. Zheng, "Nanocomposites of poly(l-lactide) and surface-grafted TiO_2 nanoparticles: synthesis and characterization," *European Polymer Journal*, vol. 44, no. 8, pp. 2476–2481, 2008.

[36] F. J. Medellín-Rodríguez, L. Larios-López, A. Zapata-Espinoza, O. Dávalos-Montoya, P. J. Phillips, and J. S. Lin, "Melting behavior of polymorphics: molecular weight dependence and

steplike mechanisms in nylon-6," *Macromolecules*, vol. 37, no. 5, pp. 1799–1809, 2004.

[37] J.-R. Sarasua, R. E. Prud'homme, M. Wisniewski, A. Le Borgne, and N. Spassky, "Crystallization and melting behavior of polylactides," *Macromolecules*, vol. 31, no. 12, pp. 3895–3905, 1998.

[38] T. Kawai, N. Rahman, G. Matsuba et al., "Crystallization and melting behavior of poly (L-lactic acid)," *Macromolecules*, vol. 40, no. 26, pp. 9463–9469, 2007.

[39] M. Yasuniwa, S. Tsubakihara, K. Iura, Y. Ono, Y. Dan, and K. Takahashi, "Crystallization behavior of poly(l-lactic acid)," *Polymer*, vol. 47, no. 21, pp. 7554–7563, 2006.

[40] D. C. Bassett, "Aspects of mechanical behavior," in *Principles of Polymer Morphology*, vol. 234, Cambridge University Press, 1981.

[41] X. Ji, J. E. Hampsey, Q. Hu, J. He, Z. Yang, and Y. Lu, "Mesoporous silica-reinforced polymer nanocomposites," *Chemistry of Materials*, vol. 15, no. 19, pp. 3656–3662, 2003.